

# Wedgebox analysis of four-lepton events from neutralino pair production at the LHC

G. Bian, M. Bisset

*Center for High Energy Physics and Department of Physics,  
Tsinghua University, P.R. China*

N. Kersting, Y. Liu, X. Wang

*Physics Department, Sichuan University, P.R. China*

## Abstract

A ‘wedgebox’ plot is a two-dimensional scatter-plot of two invariant mass quantities. Here  $pp \rightarrow e^+e^-\mu^+\mu^- + \cancel{e}$  signature LHC events are analyzed by plotting the di-electron invariant mass *versus* the di-muon invariant mass. Data sets of such events are obtained across the MSSM input parameter space in realistic event-generator simulations, including cuts designed to remove SM backgrounds. Their study reveals several general features. Firstly, regions in the MSSM input parameter space where a sufficient number of events are expected so as to be able to construct a clear wedgebox plot are delineated. Secondly, the presence of box shapes on a wedgebox plot either indicates the presence of heavy Higgs bosons decays or restricts the location to a quite small region of low  $\mu$  and  $M_2$  values  $\lesssim 200$  GeV, a region denoted as the ‘lower island’. In this region, wedgebox plots can be quite complicated and change in pattern rather quickly as one moves around in the  $(\mu, M_2)$  plane. Thirdly, direct neutralino pair production from an intermediate  $Z^{0*}$  may only produce a wedge-shape since only  $\tilde{\chi}_2^0\tilde{\chi}_3^0$  decays can contribute significantly. And fourthly, a double-wedge or wedge-protruding-from-a-box pattern on a wedgebox plot, which results from combining a variety of MSSM production processes, yields three distinct observed endpoints, almost always attributable to  $\tilde{\chi}_{2,3,4}^0 \rightarrow \tilde{\chi}_1^0\ell^+\ell^-$  decays, which can be utilized to determine a great deal of information about the neutralino and slepton mass spectra and related MSSM input parameters. Wedge and double-wedge patterns are seen in wedgebox plots in another region of higher  $\mu$  and  $M_2$  values, denoted as the ‘upper island.’ Here the pattern is simpler and more stable as one moves across the  $(\mu, M_2)$  input parameter space.

# 1 Introduction

The Large Hadron Collider (LHC) is scheduled to begin operation in less than two years, at which time the predictions of models of particle physics beyond the Standard Model (SM), especially Supersymmetry (SUSY), will be confronted with significant, and potentially lethal, experimental constraints. SUSY predicts heavy scalar counterparts, or superpartners, to the SM fermions, as well as fermionic superpartners to the SM bosons — both the spin-1 gauge bosons and the spin-0 Higgs bosons (SUSY requires more than one Higgs boson). These new states are known collectively as sparticles. Colorless sparticles, including the neutralinos ( $\tilde{\chi}_i^0$ ) and charginos ( $\tilde{\chi}_j^\pm$ ) — the neutral and charged, respectively, superpartners of admixtures of the gauge and Higgs bosons — are generally expected to be somewhat lighter than their colored brethren, the gluinos ( $\tilde{g}$ ) and squarks ( $\tilde{q}$ ). Nonetheless these latter are expected to have the largest production cross-sections, unless they are an order of magnitude or more massive. Yet this is precisely what occurs in some hypothesized SUSY-breaking scenarios: the squarks and gluinos have masses on the scale of several TeV while neutralinos and charginos have masses on the scale of several hundred GeV (or less). Therefore a study of these sparticles' direct production modes is called for. Moreover, aside from their direct production modes, colorless sparticles inevitably appear *indirectly* in any colored sparticle production process through the sometimes complicated decay chains of the gluinos and squarks. Thus, determining the masses and couplings of the neutralinos and charginos is crucial to understanding almost any SUSY events which may emerge at the LHC.

In the R-parity-conserving Minimal Supersymmetric Standard Model (MSSM), sparticles must be pair-produced, and the lightest sparticle (the LSP), for which the preferred candidate is generally the lightest neutralino ( $\tilde{\chi}_1^0$ ), is stable. The focus of this study is the neutralinos, of which there are four in the MSSM, and in particular the heavier three ( $\tilde{\chi}_i^0$ ,  $i = 2, 3, 4$  in order of increasing mass) — which are expected to decay, either directly or indirectly, into the LSP. MSSM neutralino pair production at the LHC can in general occur via three avenues herein known as: direct, Higgs-mediated, and colored-particle cascade decays, as shown in Fig. 1. Cascade decays were studied in [1], while [2] focused on Higgs-mediated decays. The present study enlarges the focus of [2] to also encompass the direct production channel via the electroweak (EW)  $Z^0$  gauge boson, which formed an unavoidable and often significant background in the [2] study. This direct avenue is most dominant when the colored sparticles and the extra Higgs bosons of the MSSM are quite massive (such as if squark, gluino, and pseudoscalar Higgs MSSM input masses are set around the TeV scale).

In an LHC detector, each short-lived heavier neutralino produced must decay into an LSP and SM particles (with the invisible LSP, and any SM neutrinos that may be present, generating the tell-tale SUSY missing energy signature). Rates for the resulting final state combinations of observed SM particles, and the distributions of the energies and momenta of said SM particles, will depend on MSSM (especially neutralino) masses and couplings. It would be simplest to examine final states that are produced by only one unique pair of neutralinos, and, on top of this, via only

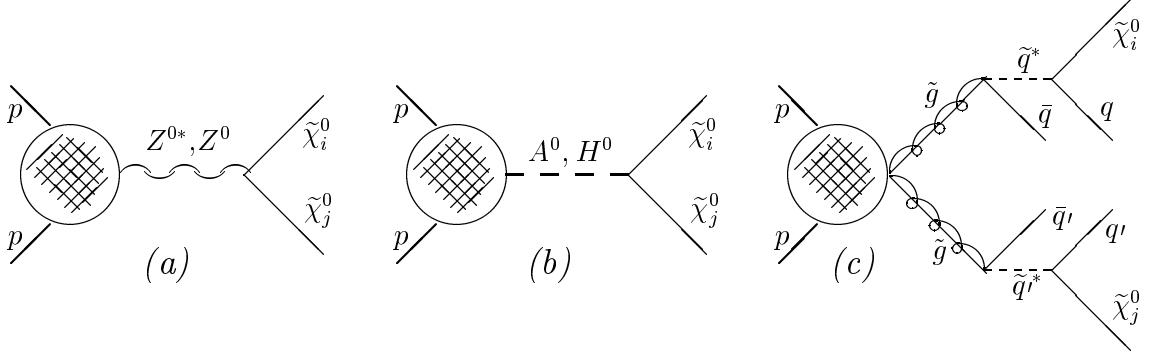


Figure 1: Feynman diagrams for heavy ( $i, j = 2, 3, 4$ ) neutralino pair production mechanisms: (a) ‘direct’ production via EW gauge boson; (b) Higgs-mediated production; and (c) production via cascade decays of gluinos (shown here) or squarks (make squarks in diagram on-mass shell and remove the gluinos and the connected quarks).

one of the aforementioned neutralino pair production avenues. Clearly though this is not a realistic expectation.

In the present study, as well as in [1], the signature examined is neutralino pair decays into an electron-positron pair, a muon-antimuon pair, and missing energy (and possibly jets):  $pp \rightarrow \tilde{\chi}_i^0 \tilde{\chi}_j^0 \rightarrow e^+ e^- \mu^+ \mu^- + \cancel{E} (+n \text{ jet})$ , where all leptons are hard and isolated (exact conditions for these requirements will be given later). The rationales for choosing this particular final state are two-fold: first, in the hadronically noisy environment of the LHC, multi-lepton signals have minimal SM backgrounds and thus tend to be easier to identify. Second, assuming the neutralinos proceed to this final state via one of the following decay chains,

$$\tilde{\chi}_i^0 \rightarrow \{Z^0, Z^{0*}\} + \tilde{\chi}_1^0 \rightarrow \ell^+ \ell^- + \tilde{\chi}_1^0 \quad (1)$$

$$\text{or} \quad \tilde{\chi}_i^0 \rightarrow \ell^\mp + \{\tilde{\ell}^\pm, \tilde{\ell}^{\pm*}\} \rightarrow \ell^+ \ell^- + \tilde{\chi}_1^0 \quad , \quad (2)$$

where  $\ell = e$  or  $\mu$ , the dilepton invariant masses are cleanly bounded by

$$0 < M_{i1}(\ell^+ \ell^-) < m_{\tilde{\chi}_i^0} - m_{\tilde{\chi}_1^0} \quad (3)$$

or

$$0 < M_{i1}(\ell^+ \ell^-) < m_{\tilde{\chi}_i^0} \sqrt{1 - \left(\frac{m_{\tilde{\ell}}}{m_{\tilde{\chi}_i^0}}\right)^2} \sqrt{1 - \left(\frac{m_{\tilde{\chi}_1^0}}{m_{\tilde{\ell}}}\right)^2} \quad , \quad (4)$$

depending on whether the decays are 3-body (via  $Z^{0*}$  or  $\tilde{\ell}^{\pm*}$ ) or 2-body via an on-mass-shell charged slepton, respectively. A 2-body decay via an on-mass-shell  $Z^0$  leads to  $M_{i1}(\ell^+ \ell^-) = M_Z$ , which is non-trivial to extract from SM backgrounds. The fact that the dilepton invariant mass spectrum basically increases as one runs up in mass to the upper kinematical edge [3] greatly facilitates a precise determination of this bound. Then, if the electron and muon pairs always come from one particular  $ij$ -combination of neutralinos, plotting their dilepton invariant masses against each other in a two-dimensional  $M(e^+ e^-)$  versus  $M(\mu^+ \mu^-)$  Dalitz-like plot [1] will yield either a box- (for  $i = j$ ) or wedge-shape (for  $i \neq j$ ) with hard kinematical edges at

(3) or (4). Note that here the lepton pairs are required to be of different flavors to facilitate proper pairings.

However, the situation is complicated at the LHC (where the partonic center-of-mass is not fixed) by the fact that several different  $ij$ -combinations may be produced — each at a different rate. Thus the plot will in general consist of a superposition of various boxes and wedges, hereafter designated as a ‘wedgebox’ plot. The power of the wedgebox plot technique manifests itself in precisely such a situation, since, given a sufficient number of events, the endpoints of (3) and (4) may each be cleanly identified, and, from the relative densities of easily-defined sectors [1] of the wedgebox plot, production ratios such as  $\sigma(pp \rightarrow \tilde{\chi}_i^0 \tilde{\chi}_j^0) / \sigma(pp \rightarrow \tilde{\chi}_k^0 \tilde{\chi}_l^0)$ , may be inferred (since the expected distribution of individual event points within a wedge or box from a particular  $ij$ -combination is fairly simple to model mathematically [3]). This information may then be used to constrain the neutralino masses and couplings and hence the fundamental MSSM input parameters (MSSM IPs) of the neutralino mass matrix. Wedgebox plots are hence superior to more traditional one-dimensional invariant mass histograms for this four-lepton signature.

Neutralino decay modes other than those included in (1) and (2) are possible. Firstly, a neutralino may not decay to the  $\tilde{\chi}_1^0$  LSP as shown in these reactions, but rather to an intermediate mass neutralino, as in  $\tilde{\chi}_4^0 \rightarrow \tilde{\chi}_3^0 + \ell^+ \ell^-$ ,  $\tilde{\chi}_4^0 \rightarrow \tilde{\chi}_2^0 + \ell^+ \ell^-$ , or  $\tilde{\chi}_3^0 \rightarrow \tilde{\chi}_2^0 + \ell^+ \ell^-$ . This additional daughter neutralino (or neutralinos) would subsequently decay to the  $\tilde{\chi}_1^0$  without producing any more leptons. The significant presence of such decay chains would introduce ‘stripes’ in the wedgebox plot, further enriching its structure: including the possibility of these stripes leads to 178 distinct<sup>1</sup> wedgebox plots within the MSSM framework. Typically though, such extended decay chains are unimportant, or at least sub-dominant. Four-lepton decays from a single neutralino  $\tilde{\chi}_i^0 \rightarrow \ell^+ \ell^- \tilde{\chi}_k^0 \rightarrow \ell^+ \ell^- \tilde{\chi}_1^0 \ell'^+ \ell'^-$  (here the aforementioned daughter neutralino does yield a lepton pair from its decay while the other production neutralino yields no leptons) are also possible, but their rates of occurrence are smaller yet. With inclusion of these stripes, and in the limit of infinite luminosity, a wedgebox plot from the LHC would consist of a  $6 \times 6$  checkerboard in the  $M(e^+ e^-) - M(\mu^+ \mu^-)$ -plane (where the location of the lines are related to the six possible mass differences between the four MSSM neutralinos). However the actual integrated luminosity of the LHC is limited, by a conservative estimate, to roughly  $300 \text{ fb}^{-1}$  over its lifetime, and generally this will not be enough to resolve the full checkerboard. Instead a specific combination of boxes and wedges will be observed in the wedgebox plot based on the dominant production modes for neutralino pairs and the dominant neutralino decay modes. Identifying these dominant modes will strongly constrain the MSSM IPs.

Secondly, and more worrisome from the point of view of the present analysis, are processes involving charginos. A neutralino may decay to the LSP via an intermediate chargino:  $\tilde{\chi}_i^0 \rightarrow \ell^+ \nu + \tilde{\chi}_1^- \rightarrow \ell^+ \nu \ell'^- \bar{\nu}' + \tilde{\chi}_1^0$ . In such decays, hereafter designated as

---

<sup>1</sup>For example,  $\tilde{\chi}_2^0 \tilde{\chi}_2^0$ ,  $\tilde{\chi}_3^0 \tilde{\chi}_3^0$  and  $\tilde{\chi}_4^0 \tilde{\chi}_4^0$  processes each separately give a box, so a wedgebox plot containing only  $\tilde{\chi}_2^0 \tilde{\chi}_2^0$  is not ‘distinct’ from a wedgebox plot containing only one of the other two processes.

‘mavericks,’ the dilepton invariant masses are not simply bounded as in reactions (3) and (4). Fortunately, such mavericks generally constitute a small minority of the events (especially for choices of the MSSM IPs which will be found to be of particular interest) leading to a diffuse ‘halo’ on a wedgebox plot which is superimposed on the desired sharp box and wedge structure. Also, the  $e^+e^-\mu^+\mu^- + \cancel{E}$  final state may result from  $\tilde{\chi}_i^\pm \tilde{\chi}_j^\mp$  chargino pair production, with  $\tilde{\chi}_i^\pm \rightarrow \ell\ell\ell'X + \tilde{\chi}_1^0$  and  $\tilde{\chi}_j^\mp \rightarrow \ell'Y + \tilde{\chi}_i^0$  (where  $X$  and  $Y$  are SM final state particles other than  $\ell$ s, typically including neutrinos, and intermediate states may involve charged sleptons or sneutrinos). Such ‘3+1’ events are also lumped into the maverick category. Thus a maverick event is any  $e^+e^-\mu^+\mu^-$  event where members of a same-flavor lepton pair arise dis-jointly rather than as in<sup>2</sup> (1) or (2). Chargino-neutralino production may yield final states with five charged leptons or four charged leptons and a charged quark pair (typically leading to jets) to balance charge. For the former, if the extra lepton is too soft or not isolated or lost down the beam pipe, or, for the latter, if a jet cut fails to exclude the event, then chargino-neutralino production may also yield  $e^+e^-\mu^+\mu^- + \cancel{E}$  events. Charginos, especially  $\tilde{\chi}_2^\pm$ , may also decay into unstable neutralinos (rather than the other way around as above):  $\tilde{\chi}_i^\pm \rightarrow \tilde{\chi}_j^0 + W^\pm \rightarrow \ell^\pm \ell'^\mp \tilde{\chi}_1^0 + q\bar{q}'$ . Here this dilepton invariant mass would fit into the expected framework, so as not to interfere with endpoint studies (though presence of such a process would skew attempts to discern neutralino pair production rates from event population studies; note also the presence of quarks that may yield unacceptable jet activity, or, if the  $W^\pm$  decays leptonically, an extra lepton would need to be lost as above). Another possibility is  $\tilde{\chi}_2^\pm \rightarrow \tilde{\nu}\ell^\pm \rightarrow \tilde{\chi}_1^0 \ell^\mp \ell^\pm \rightarrow \tilde{\chi}_1^0 \ell^\mp \ell^\pm W^\pm$  which would give kinematic edges similar to (3) or (4) (replacing  $m_{\tilde{\chi}_{1,i}^0}$  with  $m_{\tilde{\chi}_{1,2}^\pm}$  and  $m_{\tilde{\ell}}$  with  $m_{\tilde{\nu}}$ ). The presence of the above decay chains in an event would not invoke the maverick designation. Again, though, such processes are expected to have only modest rates in regions of phenomenological interest.

As noted above, colored sparticle masses may be pushed up above or around the TeV scale to prevent production rates from the cascade channel (see Fig. 1(c)) from swamping the other production modes. In [1] it was shown in full event generator level simulations that  $\sim 500$  GeV squarks and gluinos led to the overwhelming domination of the cascade channel for the  $e^+e^-\mu^+\mu^- + \cancel{E} + jets$  signature. Backgrounds were found to be nominal and signal rates high enough to produce crisp wedgebox plots over a large range of the MSSM IPs associated with neutralino characteristics. This study also showed that, as expected, jet activity is virtually always associated with cascade events. Thus a limit on the maximum number of jets or on the maximum allowable jet energy in an event can remove most of the cascade events while leaving many of the direct and Higgs-mediated events (one may speak of demanding that the events be ‘hadronically quiet’). As seen above, such a cut may also reduce the effects from maverick events.

This would leave the direct and Higgs-mediated avenues to disentangle. Note that for both these avenues the two neutralinos arise from the decay of a single fundamental particle, whereas in the cascade avenue the neutralinos are produced

---

<sup>2</sup>For ‘stripe’ events, which are not mavericks,  $\tilde{\chi}_1^0$  would be replaced by  $\tilde{\chi}_j^0$ ,  $j \neq 1$ , in (1) or (2).

independently (and possibly from decays of different colored sparticles — *e.g.*, one neutralino from a gluino and the other from a particular species of squark). Thus couplings of the EW sector of the MSSM (excluding those associated with sleptons for the moment), which are presumably determinable solely from the EW MSSM inputs to the neutralino mixing matrix, are better scrutinized via a sample of events from the direct and Higgs-mediated avenues with the cascade avenue events filtered out. Study [2] focused on the Higgs-mediated avenue and found that direct avenue production formed a background to the sought-for heavy Higgs boson signals that was difficult if not impossible to remove by any set of kinematical cuts. To focus instead on the direct channel, one could by hand simply choose the Higgs input parameter (generally chosen as the pseudoscalar Higgs mass,  $m_A$ ) large enough (in the vicinity of a TeV) to shut down the Higgs-mediated avenue. Nature may not respect this choice though. The present study avoids these dilemmas simply by not attempting to cut away either avenue: the wedgebox plot consists of a superposition of shapes from each of the two different avenues. Each avenue may contribute different shapes, if so signaling their respective presences, and, for favorable choices of the neutralino-governing MSSM IPs (as will be delineated herein), three kinematic edges — as per (3) or (4) — may be seen, strongly constraining the neutralino masses and IPs.

The remainder of the paper has the following format: in Section 2 the MSSM IP space is scanned for the inclusive rate, that is, the rate before the imposition of any kinematical cuts, of the neutralino pair-produced  $e^+e^-\mu^+\mu^- \cancel{E}$  signature via the direct and Higgs-mediated avenues to identify regions of the space where the signature is potentially observable. Guided by these estimations, Section 3 then follows with more detailed full event generator Monte Carlo (MC) simulations to carefully analyze the salient regions of the MSSM IP space. Results from the parameter space scans and the MC simulations are further expounded upon in Section 4, and finally Section 5 gives conclusions to be drawn from this work.

## 2 Parameter Space Scans

Before running a full event generator MC simulation of neutralino pair production at selected points in the MSSM IP space, it is efficient to first obtain some estimates of the typical signal and background rates. Here signal refers to direct production or Higgs-mediated avenues of neutralino pair production,  $pp \rightarrow Z^* \rightarrow \tilde{\chi}_i^0 \tilde{\chi}_j^0$  or  $pp \rightarrow H^0, A^0 \rightarrow \tilde{\chi}_i^0 \tilde{\chi}_j^0$ . If the cascade avenue is shut down either by making the colored sparticles very massive or by an appropriate jet cut, then the main MSSM backgrounds are from chargino and slepton production. Processes not studied in this initial analysis therefore include minor players such as  $t\bar{t}h$ ,  $tH^\pm$ ,  $tbH^\pm$ , *etc.*, and all SM backgrounds. Though these all may lead to a  $e^+e^-\mu^+\mu^- + \cancel{E}$  signature, it was shown in MC studies [2] that they contribute negligibly after a suitable set of cuts (namely the ones we will employ in this work): in particular SM processes may be virtually eliminated by demanding a sufficient amount of missing energy, hard leptons that are isolated, and limits on jet activity — save for  $Z^0 Z^{0*}$ -induced events, which lead to a few dozen events along the ‘Z-lines’ on a wedgebox plot; so at worst

these lead to Z-line enhancement.

The MSSM IPs that factor directly in the neutralino and chargino mixing matrices are  $\tan\beta$ , the ratio of the Higgs boson vacuum expectation values,  $\mu$ , the SUSY higgsino mass parameter, and  $M_2$ , the soft SUSY-breaking  $SU(2)_L$  gaugino mass (in what follows,  $M_1$ , the soft SUSY-breaking  $U(1)_Y$  gaugino mass, is assumed to be fixed by  $M_2$  and the gauge unification constraint  $M_1 = 5/3 \tan^2\theta_W M_2$ ). These MSSM IPs are allowed to take values in the ranges:  $2 < \tan\beta < 50$  (upper limit guided by perturbativity), and  $100 \text{ GeV} < \mu, M_2 < 500 \text{ GeV}$  — here the lower bound is set to avoid LEP-excluded light colorless sparticles and the upper bound to avoid heavier neutralinos ( $\tilde{\chi}_3^0$  and  $\tilde{\chi}_4^0$ ) too massive to generate significant production rates.

Higgs-mediated events are sensitive to the pseudoscalar Higgs mass  $m_A$ : as  $m_A$  increases, phase space opens up for more  $\tilde{\chi}_i^0 \tilde{\chi}_j^0$  decay channels; however, the cross section for  $pp \rightarrow H^0, A^0$  drops precipitously. Thus the preferred range for a potentially meaningful contribution from the Higgs-mediated avenue is  $300 \text{ GeV} \lesssim m_A \lesssim 700 \text{ GeV}$ .

Also of crucial importance to the neutralino decays into charged leptons are the slepton sector MSSM IPs. Each flavor generation has two soft slepton mass inputs  $m_{\tilde{\ell}_{L,Ri}}$  ( $i = e, \mu, \tau$ )<sup>3</sup> Most models of SUSY breaking generate little splitting between the inputs of the first two generations, and thus, for simplicity, these inputs are set degenerate. This assumption makes the wedgebox plots virtually symmetric under the interchange of the axes, while relaxing this assumption may make the wedgebox plot asymmetric (for instance, the ‘boxes’ could become ‘rectangles’). The third generation stau inputs are however distinctive in many SUSY-breaking scenarios, and herein these inputs are elevated (by hand) by 100 GeV over the degenerate selectron and smuon mass inputs. The lighter selectrons and smuons then favor, via reaction (2), events of the signature type over those containing tau leptons. This enhances the signal rates while at the same time reducing one additional source of maverick events (stemming from events with leptonic tau decays). Conversely, measuring the asymmetry and maverick halo density of the observed wedgebox plot would provide information about the slepton sector mass inputs. This leaves two parameters from the slepton sector to vary: the degenerate soft SUSY-breaking mass input for the right sleptons of the first two generations (the superpartners of the right-handed electron and muon),  $m_{\tilde{\ell}_R}$ , and the corresponding mass input for the left sleptons,  $m_{\tilde{\ell}_L}$ . If both these slepton masses are set very high, then neutralino decays via gauge bosons as in reactions (1) totally dominate and the leptonic branching ratios (BRs) of the neutralinos are simply those of the SM gauge bosons. This is insufficient for generating enough events for detection of the signature. Thus positive results in this work depend on sleptons being reasonably light ( $\lesssim 350 \text{ GeV}$ ) — a condition that fits comfortably with the neutralino MSSM IPs under consideration. These light sleptons will then enhance the leptonic BRs of the neutralinos [4]. In addition to generating reactions like (2), light slepton mass inputs can also generate

$$\tilde{\chi}_i^0 \rightarrow \bar{\nu} + \tilde{\nu} \rightarrow \bar{\nu}\nu + \tilde{\chi}_1^0 \quad (5)$$

---

<sup>3</sup>There are also trilinear soft inputs  $A_{\ell i}$ , but these always come attached to a Yukawa coupling and thus are irrelevant for the first two generations.

decay chains which act as spoiler modes to kill the  $4\ell$  signal. If  $m_{\tilde{\nu}} < m_{\tilde{\chi}_2^0} < m_{\tilde{\ell}^\pm}$ , then  $\tilde{\chi}_2^0$  mainly decays via an on-shell sneutrino and its BR into a pair of charged leptons is highly suppressed. If SUSY-breaking processes respect  $SU(2)_L$  symmetry, then the sneutrino and left charged lepton of a given flavor have the same soft input mass parameter; however, D-terms break this degeneracy to a limited extent. Since the sneutrino mass is thus tied to  $m_{\tilde{\ell}_L}$ , lowering  $m_{\tilde{\ell}_R}$  relative to  $m_{\tilde{\ell}_L}$  tends to improve the signal rate.

A private code was used normalized by cross-sections input from the event generator ISAJET [5] to perform a scan over the  $\mu$  and  $M_2$  neutralino IPs for the signature  $\sigma(pp \rightarrow X) \times B.R.(X \rightarrow e^+e^-\mu^+\mu^-)$  where  $X$  represents the intermediate states (as in Fig. 1 (a) or (b) in the case of the signal). Other MSSM IPs were fixed as follows:  $\tan\beta = 10$ ,  $m_A = 600$  GeV,  $m_{\tilde{g},\tilde{q}} = 1000$  GeV,  $m_{\tilde{e},\tilde{\mu}} = 150$  GeV,  $m_{\tilde{\tau}} = 250$  GeV, and vanishing soft  $A$ -terms. In this initial parton-level analysis, the mere presence of exactly the four leptons in the signature is all that is required with no demands whatsoever made upon their kinematical properties (*e.g.*, transverse momenta or pseudorapidity). Any effects from the underlying spectator event are neglected. By contrast, in the full event generator MC analysis to follow appropriate cuts on the leptons' kinematical properties will be applied, meaning that the numerical results of the initial analysis are over-estimates. The initial analysis also demands no quarks in the final state, where only particles resulting from the primary parton-level interaction are taken into account. On the other hand, in the full event generator MC analysis at the very least quark remnants from the colliding protons must yield quarks in the final state (though these typically lie close to the beam axis). Thus at best a lower bound can be set upon hadronic or jet activity in the final state, which would tend to make the results of the initial analysis under-estimates of the event generator MC results. Of these two differences between the two analyses, the former effect is expected to be more significant. Thus the results from the initial analysis may be treated as upper bounds of what may be expected from the more thorough event generator MC studies.

Fig. 2 shows the results<sup>4</sup>, assuming an integrated luminosity of  $100\text{ fb}^{-1}$ . The lower and upper shaded areas are excluded by LEP searches (restricting<sup>5</sup>  $m_{\tilde{\chi}_1^\pm}$ ) and cosmological/dark matter considerations (*i.e.*, require  $\tilde{\chi}_1^0$  to be the LSP), respectively. Plot (a) shows what may be expected from the direct channel. Of the six possible  $\tilde{\chi}_i^0\tilde{\chi}_j^0$  pairs ( $i, j = 2, 3, 4$ ), only the  $\tilde{\chi}_2^0\tilde{\chi}_3^0$  combination leads to a significant number of events (set as 100 events). Phase space suppression renders the  $\tilde{\chi}_i^0\tilde{\chi}_4^0$  channels negligible. The rate for  $\tilde{\chi}_2^0\tilde{\chi}_2^0$  is suppressed since, in the pertinent region of the  $\mu$ ,  $M_2$

<sup>4</sup>Note that in this plot, as well as other to follow  $\mu > 0$  is chosen. While analogous plots for  $\mu < 0$  are not quite symmetric to the  $\mu > 0$  plots shown here, substantive differences are few with the same features appearing at slightly shifted values of  $|\mu|$ .

<sup>5</sup>For physical sneutrino masses below 200 GeV, destructive interference from a  $t$ -channel sneutrino exchange diagram with the normal  $s$ -channel diagram for  $e^+e^-$ -collider chargino pair production lowers the bound given by LEP experimental groups [6] from  $m_{\tilde{\chi}_1^\pm} > 103$  GeV (singly hatched bound on plots) to  $m_{\tilde{\chi}_1^\pm} > 85$  GeV (doubly hatched bound on plots). A true experimentalist's bound for the MSSM IP sets considered herein would thus be expected to lie somewhere within the singly hatched zone.



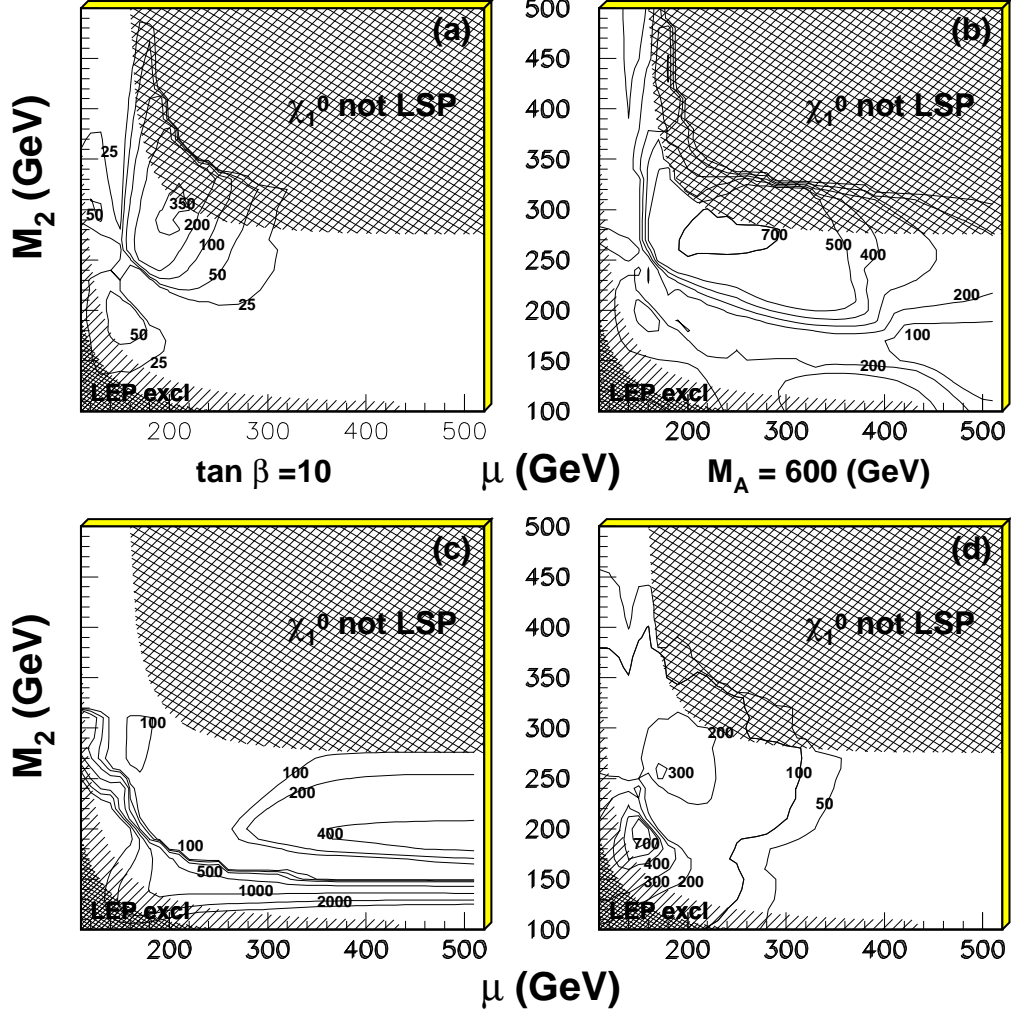


Figure 2: Number of  $e^+e^-\mu^+\mu^-$  events (inclusive rates with no cuts) expected per  $100\text{fb}^{-1}$  of integrated luminosity from (a)  $pp \rightarrow \tilde{\chi}_2^0\tilde{\chi}_3^0$ ; (b)  $pp \rightarrow H^0/A^0$ ; (c)  $pp \rightarrow \tilde{\chi}_i^0\tilde{\chi}_j^\pm$  and (d)  $pp \rightarrow \tilde{\chi}_i^\pm\tilde{\chi}_j^\mp$ . Other MSSM inputs are fixed as  $\tan\beta = 10$ ,  $m_A = 600\text{ GeV}$ ,  $m_{\tilde{e},\tilde{\mu}} = 150\text{ GeV}$  and  $m_{\tilde{\tau}} = 250\text{ GeV}$ . The uncertainty shown in the extent of the LEP excluded region stems from the presence of a relatively light sneutrino (as discussed in a footnote).

parameter space, the  $\tilde{\chi}_2^0$  has approximately equal higgsino components and the  $Z\tilde{\chi}_2^0\tilde{\chi}_2^0$  coupling<sup>6</sup> vanishes due to the cancellation between the contributions from these two higgsino components. An analogous suppression occurs with the  $\tilde{\chi}_3^0\tilde{\chi}_3^0$  mode, along with substantial phase space suppression. Note that there are too few events at

<sup>6</sup>In the notation of [7], this term is  $\langle Z|\tilde{\chi}_i^0\tilde{\chi}_j^0\rangle = (g/2\cos\theta) \text{Re}(N_{i3}N_{j3}^* - N_{i4}N_{j4}^*)$ . The crucial minus sign in this equation arises from the different hypercharges of the two MSSM Higgs doublets. If  $i = j$ , this leads to a strong tendency for the two terms to cancel each other. However, for  $i = 2$  and  $j = 3$ , as in direct  $\tilde{\chi}_2^0\tilde{\chi}_3^0$  production, the signs of either  $N_{23}$  and  $N_{33}$  or  $N_{24}$  and  $N_{34}$  — but not both — are opposite over much of the interesting region of the MSSM IP space, and enhancement rather than cancellation ensues.

either high  $M_2$  and/or high  $\mu$  to meet the significance criterion due to the small size of  $\sigma(pp \rightarrow \tilde{\chi}_2^0 \tilde{\chi}_3^0)$ . In the remaining portion of the plane sneutrino spoiler modes — which confound  $\tilde{\chi}_2^0 \rightarrow \ell^+ \ell^- \tilde{\chi}_1^0$  decays — carve out a valley in the event-rate topology, seen in the  $(\mu, M_2)$  MSSM IP plane as a more or less hyperbolic swath passing through  $(\mu, M_2) = (200 \text{ GeV}, 200 \text{ GeV})$ , leaving two peaks at  $(\mu, M_2) \simeq (200 \text{ GeV}, 300 \text{ GeV})$  and  $(150 \text{ GeV}, 175 \text{ GeV})$ <sup>7</sup>.

Plot (b) gives the results for the Higgs-mediated channels. Rates everywhere exceed those of the direct  $\tilde{\chi}_2^0 \tilde{\chi}_3^0$  production mode since the mechanism suppressing  $\tilde{\chi}_2^0 \tilde{\chi}_2^0$  in the direct channel does not apply to the Higgs' couplings. However the optimal point in the plane is in roughly the same location, around  $(\mu, M_2) \simeq (200 \text{ GeV}, 275 \text{ GeV})$ . This is strongly influenced by the aforementioned sneutrino spoiler mechanism choking off the event rate as one moves off this peak. These features directly follow from the choices made for  $m_A$  and  $\tan \beta$  (600 GeV and 10, respectively). As found in [2], Higgs decays to  $\tilde{\chi}_2^0 \tilde{\chi}_2^0$  tend to dominate for larger values of  $\mu$ . This means that Higgs-mediated processes can lead to a box, whereas the direct avenue is expected to produce a wedge. On the other hand, [2] also found that decays including the heavier neutralinos  $\tilde{\chi}_3^0$  and  $\tilde{\chi}_4^0$  may be very significant or even dominate for smaller values of  $\mu$  (assuming  $m_A$  is sufficiently large). Thus more complicated wedgebox plots may be expected from Higgs-mediated processes at lower values of  $\mu$  (and higher values of  $m_A$ ).

The most significant SUSY backgrounds involve charginos. Plots (c) and (d) of Fig. 2 display expected 5- and 4-lepton event rates from  $pp \rightarrow \tilde{\chi}_i^0 \tilde{\chi}_j^\pm$  and  $pp \rightarrow \tilde{\chi}_i^\pm \tilde{\chi}_j^\mp$ , respectively. Here the  $\tilde{\chi}_i^0 \tilde{\chi}_j^\pm$  pair is required to produce five leptons, and then one lepton would have to be ‘lost.’ Losing the extra lepton is *not* taken into account in the rates shown in (c), and thus rates shown for this process are certainly considerably over-estimated. Nonetheless, the plot clearly shows that the largest rates from  $\tilde{\chi}_i^0 \tilde{\chi}_j^\pm$  should come at low values of  $M_2$  (with some preference also for higher values of  $\mu$ ). This is not a region where the direct and Higgs-mediated neutralino-pair production processes are expected to yield enough events to sufficiently populate a wedgebox plot. Thus at worst  $\tilde{\chi}_i^0 \tilde{\chi}_j^\pm$  processes would contribute a small minority of the events in a neutralino-pair-induced wedgebox plot. As seen from plot (d), chargino pair production is expected to generate a fair number of four lepton events (typically mavericks) which might act to cloud the neutralino-based features of the wedgebox plot. Light charginos are generally expected to have larger cross-sections at the LHC than neutralinos. Fortunately,  $\tilde{\chi}_1^+ \tilde{\chi}_1^-$ -production can almost never generate the four-lepton final state. Requiring processes involving the heavier chargino pushes the location for optimal rates from chargino-pair production to quite low values of  $M_2$  and  $\mu$ . This is mostly non-overlapping with the sweet spot for neutralino-pair-production processes; however, a secondary maxima in the chargino-pair rates is seen at  $(\mu, M_2) \simeq (200 \text{ GeV}, 250 \text{ GeV})$ , and this is in the region where a neutralino-pair-induced wedgebox plot would be viable. One possible method for alleviating

---

<sup>7</sup>Though not very discernible on the plots, there is also a very narrow bridge of high rates centered on  $(\mu, M_2) \simeq (155 \text{ GeV}, 245 \text{ GeV})$ . This is where the sneutrino coupling to  $\tilde{\chi}_2^0$  dies, turning off the most important spoiler mode.

this problem (not implemented in this work) would be to examine  $\ell^+\ell^-\ell^+\ell'^-$  events (since with  $\tilde{\chi}_i^+\tilde{\chi}_j^-$  one chargino is expected to produce three leptons while the other chargino produces only one, while with  $\tilde{\chi}_i^0\tilde{\chi}_j^0$  each neutralino should, with rare exceptions, produce a pair of same-flavor leptons), which should have rates equivalent to  $\ell^+\ell^-\ell^+\ell^-$ , as the basis for a chargino-pair event subtraction scheme [8].

Finally, slepton production also comprises a potentially large background. In [2], four-lepton signature events from slepton-pair production were found to be even harder to cut away from the desired Higgs-mediated signal than events from direct avenue neutralino pair production, though in that case only enough Higgs-mediated signal events were sought to claim a signal of  $\sim 20$  events after all cuts. In this work, on the other hand, hundreds of events are needed. We discuss this issue at more length in the following section, where it is found that sleptons contribute significantly only at very low values of  $\mu$  or  $M_2$ ; *i.e.*, in regions where signal rates are small. However, sleptons are always of paramount importance as intermediates in the decays of the neutralinos to the desired charged leptons.

### 3 Monte Carlo Event Generator Analysis

The HERWIG 6.5 [9] MC package (which obtains its MSSM input information from ISASUSY [5] through the ISAWIG [11] and HDECAY [12] interfaces) is employed to generate realistic LHC events. The CTEQ 6M [10] set of parton distribution functions is used with top and bottom quark masses set to  $m_t = 175 \text{ GeV}$  and  $m_b = 4.25 \text{ GeV}$ , respectively. This is coupled with private programs simulating a typical LHC detector environment (these codes have been checked against results in the literature). Assuming an integrated luminosity of  $100 \text{ fb}^{-1}$ , roughly equivalent to the first few years' data at the LHC, the appropriate numbers of events (normalization was according to HERWIG-delivered cross-sections) for signal and background processes were generated at an array of points spanning the  $(\mu, M_2)$  plane.

Signature  $e^+e^-\mu^+\mu^-$  events are selected according to the following criteria: the event must have exactly four hard ( $p_T^\ell > 10, 8 \text{ GeV}$  for  $e^\pm, \mu^\pm$ , respectively), isolated (no tracks of other charged particles in a  $r = 0.3$  radians cone around the lepton, and less than  $3 \text{ GeV}$  of energy deposited into the electromagnetic calorimeter for  $0.05 \text{ radians} < r < 0.3 \text{ radians}$  around the lepton) leptons, consisting of exactly one  $e^+e^-$  pair and one  $\mu^+\mu^-$  pair.

After identifying signature events, the following cuts are then applied:

- Substantial missing transverse energy must be present, with  $20 \text{ GeV} < \cancel{E}_T < 130 \text{ GeV}$ , and
- No jet reconstructed with an energy  $E_{jet}$  greater than  $50 \text{ GeV}$ .

Jets are defined by a cone algorithm with  $r = 0.4$  and must have  $|\eta^j| < 2.4$ . These cuts are sufficient to eliminate all of the SM backgrounds except that from  $Z^0 Z^{0*}$  production. Gluino and/or squark pair production events are also removed, leaving only residual SUSY backgrounds from processes involving charginos ( $pp \rightarrow \tilde{\chi}_i^\pm \tilde{\chi}_j^\pm$  or  $\tilde{\chi}_i^0 \tilde{\chi}_j^\pm$  via SM gauge bosons or Higgs bosons), from charged slepton pair production ( $pp \rightarrow \tilde{\ell}^\pm \tilde{\ell}^\mp$ ), and (making a minor contribution) from  $pp \rightarrow tH^-, \bar{t}H^+$ .

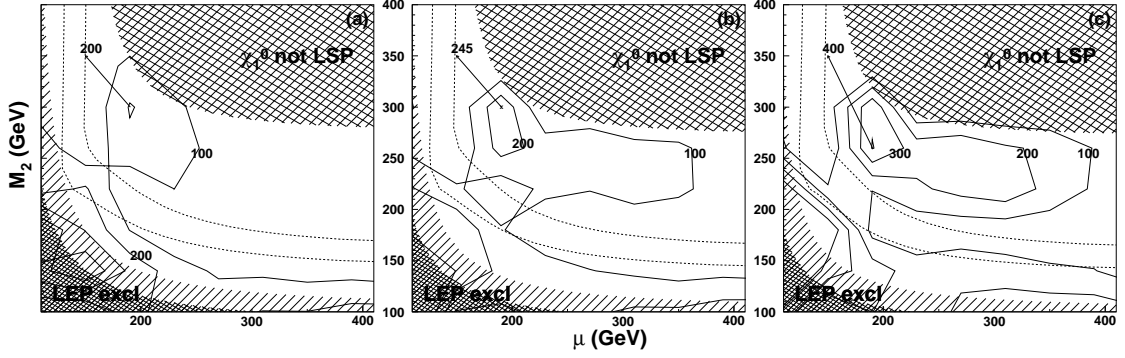


Figure 3: Number of  $e^+e^-\mu^+\mu^-$  events (event generator simulated, after cuts) at  $\tan\beta = 5$  (left),  $\tan\beta = 10$  (middle), and at  $\tan\beta = 20$  (right);  $m_A = 600$  GeV,  $m_{\tilde{\ell}_L} = m_{\tilde{\ell}_R} = 150$  GeV ( $\ell = e, \mu$ ) and  $m_{\tilde{\tau}} = 250$  GeV. Assuming an integrated luminosity of  $100 \text{ fb}^{-1}$ . Region between the two hyperbolic dashed curves is where the sneutrino spoiler modes cut heavily into event rates.

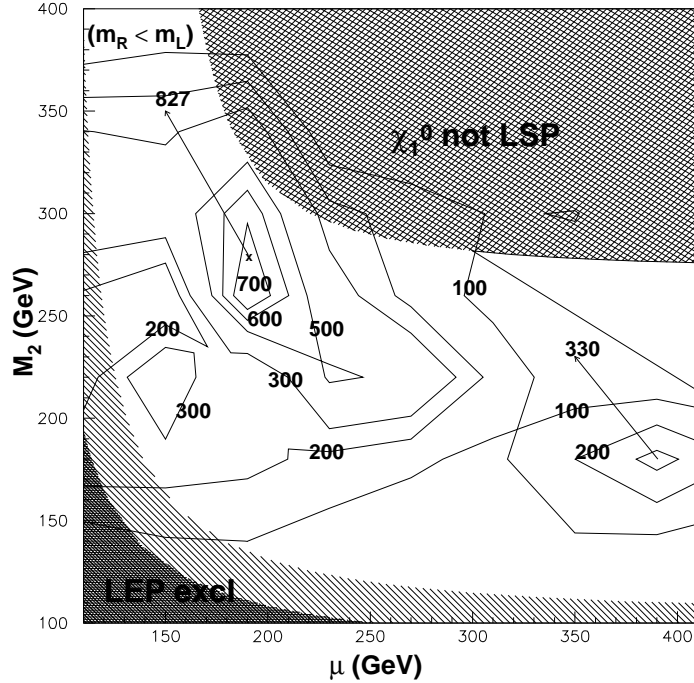


Figure 4: Number of  $e^+e^-\mu^+\mu^-$  events (event generator simulated, after cuts) with  $\tan\beta = 10$ ,  $m_{\tilde{\ell}_L} = 200$  GeV and  $m_{\tilde{\ell}_R} = 150$  GeV ( $\ell = e, \mu$ ) and  $m_{\tilde{\tau}} = 250$  GeV;  $m_A = 600$  GeV. Assuming an integrated luminosity of  $100 \text{ fb}^{-1}$ .

Fig. 3 shows contour plots in the  $(\mu, M_2)$ -plane of the number of events, due to the combined signal and background processes given in Fig. 2 (plus the slepton background), expected to pass the above set of cuts, assuming an integrated luminosity of  $100 \text{ fb}^{-1}$ . Two ‘islands’ where the number of expected events swell to over 100 appear. As expected, rates are down (roughly by factors of from two to four) from the

bounding estimates given Fig. 2, but the general features match well those expected based on the parameter space scan. The location of the upper island corresponds fairly well with the locations of the maxima from direct and Higgs-mediated neutralino pair production in Fig. 2. Also according to Fig. 2, the lower island, which is partially covered by the LEP excluded region, is situated where both the direct and Higgs-mediated signal processes *and* the chargino-related background processes produce substantial numbers of events. The numbers in Fig. 2 would seem to indicate that the lower island should be totally dominated by chargino-related events; however, recall that plot (c) in that figure does not take into account the fraction of the time the extra fifth lepton from  $pp \rightarrow \tilde{\chi}_i^0 \tilde{\chi}_j^\pm$  is lost. After cuts, signal and background rates on this lower island are found to be comparable, though chargino-related plus slepton background events still typically contribute a majority of the events. In particular, in a thin strip of points hugging the  $\mu$  axis slepton pair production, which yields four leptons via a ‘3+1’ process,

$$\begin{aligned} \tilde{\ell}^\pm &\rightarrow \ell'^\pm \tilde{\chi}_2^0 \rightarrow \ell'^\pm \ell^\mp \ell^\pm \tilde{\chi}_1^0 \\ \tilde{\ell}^\mp &\rightarrow \ell'^\mp \tilde{\chi}_1^0 \end{aligned} \quad (6)$$

yields almost all the events since direct and Higgs-mediated modes are cut back by increasingly heavy neutralino masses. A corresponding strip also extends along the  $M_2$  axis, but here sleptons prefer to decay to  $\tilde{\chi}_3^0$  until it becomes kinematically more favorable to decay to charginos ( $m_{\tilde{\chi}_3^0} > m_{\tilde{\ell}^\pm} > m_{\tilde{\chi}_1^\pm}$ ) which do not yield the desired 4-lepton final state; therefore for the particular slepton masses employed in these scans this strip terminates near  $M_2 \sim 300$  GeV. The plots in Fig. 3 also illustrate that rates around the upper island in the  $(\mu, M_2)$  plane rise with  $\tan\beta$ ; mostly this is due to an accompanying increase in the Higgs bosons’ production rates – Higgs-mediated events rise from less than 10% of the total at  $\tan\beta = 5$  to 60% at  $\tan\beta = 20$  — but  $\tan\beta$ -induced changes in the neutralino & chargino masses and couplings also play a role. If the SUSY-breaking stau mass inputs are set equal to or slightly above the inputs of the first two slepton generations, then rates of all signal processes will fall precipitously after some high  $\tan\beta$  limit is reached. This is due to mixing in the stau sector driving down one of the physical stau masses leading to sparticle and heavy Higgs boson decays predominantly filled with tau-leptons. The complex interplay of  $\tan\beta$  with the observed masses and couplings underscores the difficulty in going from an observed number of events to predictions for MSSM IP values. Note however that the gross appearance and location of the maxima/‘islands’ where a sufficient number of events are produced is little altered.

Note also the continued appearance of the hyperbolic swath in the  $M_2$  vs.  $\mu$  plots. As in Fig. 2, this is caused by sneutrino spoiler modes which are expected to dominate in the region between the dotted lines in Fig. 3. The strength of said spoiler modes varies with the input slepton mass parameters chosen. These include (see [1]):  $\tan\beta$ , trilinear soft  $A$ -terms whose effects are insignificant for the first two generations, and the soft slepton mass inputs. Results with the canonical choice of  $m_{\tilde{\ell}_L} = m_{\tilde{\ell}_R} = 150$  GeV (used in all of the other figures presented in this work) seen in the center ( $\tan\beta = 10$ ) plot of Fig. 3 may be compared to those from elevating

$m_{\tilde{\ell}_L}$  to 200 GeV in Fig. 4. Elevating  $m_{\tilde{\ell}_L}$  raises the physical sneutrino masses (as well as the masses of the left charged sleptons) above those of the right charged sleptons, choking off the spoiler modes. Comparing the two results, we see that the rates when  $m_{\tilde{\ell}_L}$  is made heavier actually increase, despite the diminution of the left charged slepton channel, and the swath of low event rates that was cutting across the plot has now largely vanished, allowing a third maximum to surface near  $(M_2, \mu) = (390 \text{ GeV}, 180 \text{ GeV})$ . This third peak is almost entirely due to Higgs-mediated  $H^0/A^0 \rightarrow \tilde{\chi}_2^0 \tilde{\chi}_{2,3}^0$  modes (direct modes' cross-sections are too small here): as one moves off this peak to lower  $M_2$  or  $\mu$ , intermediate sleptons become off-shell and suppress  $\tilde{\chi}_2^0 \rightarrow \ell^+ \ell^- \tilde{\chi}_1^0$  decays, whereas moving to higher values of these parameters raises the masses of  $\tilde{\chi}_{2,3}^0$  and thus suppresses  $H^0/A^0 \rightarrow \tilde{\chi}_2^0 \tilde{\chi}_{2,3}^0$  modes.

The foregoing demonstrates that regardless of the values of  $\tan\beta$ ,  $M_A$ , and the slepton masses<sup>8</sup>, there are always two disjoint regions of high (over 100 events per  $100 \text{ fb}^{-1}$ ) rates in the  $(M_2, \mu)$  plane. Let us now examine what, if any, pattern there is to the wedgebox plots in these regions. Taking for definiteness  $\tan\beta = 20$  (right plot of Fig. 3), wedgebox plots are generated at an array of  $(\mu, M_2)$  points, assuming an integrated luminosity of  $300 \text{ fb}^{-1}$ , to obtain the ‘wedgebox map’ shown in Fig. 5. Each symbol in the wedgebox map represents a shape ascertained from visual inspection of the corresponding wedgebox plot (explicit examples are forthcoming) at that point. Based upon an LHC integrated luminosity of  $300 \text{ fb}^{-1}$ , this wedgebox map represents the potential of the LHC to correlate neutralino MSSM IPs  $\mu$  and  $M_2$  with an observed wedgebox shape if Nature has chosen  $\tan\beta = 20$ ,  $M_A = 600 \text{ GeV}$ ,  $m_{\tilde{g}, \tilde{q}} = 1000 \text{ GeV}$ , and  $m_{\tilde{\ell}_{L,Ri}} = 150 \text{ GeV}$  ( $i = e, \mu$ ),  $250 \text{ GeV}$  ( $i = \tau$ ). Fig. 5 is thus a representative example of a class of  $(\mu, M_2)$  wedgebox plots that can be made by varying these additional inputs.

Toward the lower left-hand corner of Fig. 5, in the region of the lower island, one sees a fairly complicated evolution of shapes, as might be expected since here the direct, Higgs-mediated, chargino-related and slepton-pair production modes all contribute significantly. For example, the wedgebox pattern for the point  $(\mu, M_2) = (150 \text{ GeV}, 160 \text{ GeV})$  is depicted in Fig. 5 as a box with a wedge extending out of it. The actual wedgebox plot is shown in Fig. 6(a). A sizable fraction of the events are chargino-related mavericks (*vis à vis* Secn. 1). While some kinematical edges are clearly visible, the high fraction of mavericks makes it especially difficult to connect these with mass differences in the neutralino spectrum. For example, the clustering of points near 45 GeV is in fact a mixture of the  $\tilde{\chi}_2^0 \rightarrow \tilde{\chi}_1^0$  decay edge through an off-shell slepton ( $M_{21}(\ell^+ \ell^-) = 45.7 \text{ GeV}$ ) and the  $\tilde{\chi}_3^0 \rightarrow \tilde{\chi}_1^0$  edge through on-shell sleptons ( $32.5 \text{ GeV} < M_{31}(\ell^+ \ell^-) < 45.5 \text{ GeV}$ )<sup>9</sup>. The large width of  $M_{31}$  here is due

<sup>8</sup>Assuming these are less than  $\sim 300 \text{ GeV}$ , otherwise event rates are too low.

<sup>9</sup>Here it is necessary to make note of a small inadequacy in the analysis package used to generate the wedgebox plots: a term in the slepton masses from left-right sfermion mixing — the  $m_{\tilde{\ell}}^2 \mu^2 \tan^2 \beta$  term in Eqn. (13) of [1] — is neglected in ISASUSY 7.58 [5] which feeds the mass values into HERWIG 6.5 [9]. Neglecting this term, the mass splitting of the smuons becomes equal to that of the selectrons, and thus is evidently sometimes under-estimated. Numerical values given in the text correctly account for this term, and so may not exactly correspond to what is observed in the wedgebox plot figures, though the differences are not crucial to the current analysis and discussion.

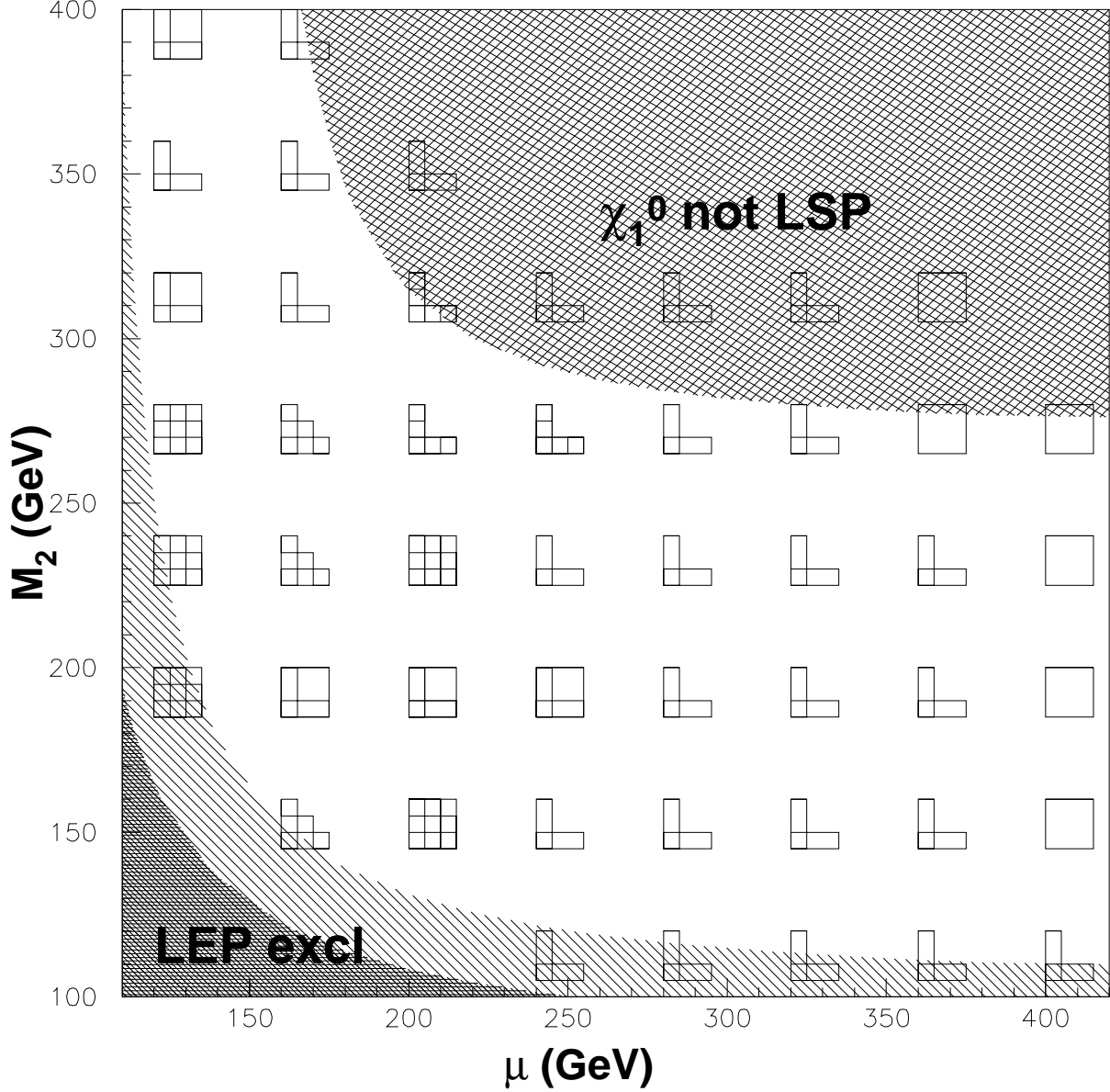


Figure 5: Wedgebox ‘map’ for  $\tan\beta = 20$  and assuming an integrated luminosity of  $300\text{ fb}^{-1}$ . Idealized wedgebox plot patterns abstracted from visual inspections of wedgebox plots obtained from simulation runs at an array of points spanning the parameter space. Values of other fixed parameters:  $m_A = 600\text{ GeV}$ ,  $m_{\tilde{g},\tilde{q}} = 1000\text{ GeV}$ , and  $m_{\tilde{\ell}_{L,Ri}} = 150\text{ GeV}$  ( $i = e, \mu$ ),  $250\text{ GeV}$  ( $i = \tau$ ). The uncertainty shown in the extent of the LEP excluded region stems from the presence of a relatively light sneutrino (as discussed in an earlier footnote).

to the proximity of the slepton masses to that of  $\tilde{\chi}_3^0$ . Moreover, the edge seen near 115 GeV arises not from a neutralino decay, but from  $\tilde{\chi}_2^\pm \rightarrow \tilde{\nu} \ell^\pm \rightarrow \tilde{\chi}_1^\pm \ell^\pm \ell^\mp$ : this decay yields two leptons with an invariant mass cutoff of 118.7 GeV determined by the charginos' mass difference. Not easily discernible in the plot is another edge from  $\tilde{\chi}_4^0 \rightarrow \tilde{\chi}_1^0$  decays (calculated as  $141.8 \text{ GeV} < M_{41}(\ell^+ \ell^-) < 144.6 \text{ GeV}$ ); these mostly arise from Higgs-mediated events. Finally, the long tail of events along the axes arises from the slepton background, since at these small values of  $\mu$  and  $M_2$  the '3+1' decay modes (see (7)) open: a hallmark of the '3+1' modes is a wedge with a diffuse tail extending to high invariant masses, since one lepton pair will have a well-defined invariant mass cutoff (usually  $m_{\tilde{\chi}_2^0} - m_{\tilde{\chi}_1^0}$ ) while the other pair will not. The multitude of significant source processes for the event points, the quick evolution of wedgebox patterns as one moves around the  $(\mu, M_2)$  plane, and the strong contingent of maverick events all make this a tricky region of the MSSM IP space to analyze via the methodology adopted here. On the other hand, a sufficiently complicated wedgebox plot may indicate that Nature has chosen a point in this relatively small (especially given the portion ruled out by LEP) sector of the IP space.

As one moves to higher values of  $\mu$  and  $M_2$ , the wedgebox shapes become much less sensitive to small shifts in the  $(M_2, \mu)$  plane. In the region of the upper island the wedgebox pattern almost exclusively consists of either a wedge, a 'double-wedge,' or a box. This is primarily because the chargino-related production modes are far weaker in this region, and thus the dominant source of events is direct neutralino pair production, which as stated earlier is basically just  $\tilde{\chi}_2^0 \tilde{\chi}_3^0$  production, along with Higgs-mediated neutralino pair production. In fact at sufficiently high values of  $M_2$  or  $\mu$  only this latter contributes via  $H^0/A^0 \rightarrow \tilde{\chi}_2^0 \tilde{\chi}_2^0$ , giving a simple box shape. In the interior of the upper island direct  $\tilde{\chi}_2^0 \tilde{\chi}_3^0$  production yields one wedge with an inner (outer) edge at  $M_{i1}(\ell^+ \ell^-)$  for  $i = 2(3)$ . Significant Higgs-mediated modes in this region are  $H^0/A^0 \rightarrow \tilde{\chi}_2^0 \tilde{\chi}_2^0$ ,  $\tilde{\chi}_2^0 \tilde{\chi}_3^0$  and  $\tilde{\chi}_2^0 \tilde{\chi}_4^0$ . However, for most points on the upper island the crucial  $\tilde{\chi}_2^0 \tilde{\chi}_4^0$  contribution is too faint to give a distinct edge, and the other Higgs processes will simply reinforce the kinematical edges<sup>10</sup> from  $\tilde{\chi}_2^0 \tilde{\chi}_3^0$  production, yielding a single wedge. However near the maximum of this island at  $(M_2, \mu) = (190 \text{ GeV}, 280 \text{ GeV})$  the  $\tilde{\chi}_2^0 \tilde{\chi}_4^0$  contribution is substantial and a second wedge extends out from the first with an inner (outer) edge at  $M_{i1}(\ell^+ \ell^-)$  for  $i = 2(4)$ ; giving a 'double-wedge.'

In the special region where a double-wedge pattern is observed, one can unambiguously identify the quantities  $M_{i1}(\ell^+ \ell^-)$  ( $i = 2, 3, 4$ ) which will put significant constraints on the neutralino and physical slepton masses; these in turn determine the MSSM IPs  $M_1$ ,  $M_2$ ,  $\mu$ ,  $\tan \beta$  and  $m_{\tilde{e}_{L,R}}$ ,  $m_{\tilde{\mu}_{L,R}}$ . Fig. 6(b) shows the MC simulation of the double-wedge at  $(\mu, M_2) = (190 \text{ GeV}, 280 \text{ GeV})$ . As both direct and Higgs-mediated modes contribute nearly 500 events each at this point, the approximate locations of the three kinematic edges are easily visible. Unfortunately, as a practical matter high rates such as these are indispensable in comfortably distinguishing a double-wedge from the more common (across the parameter space) single-wedge wedgebox plots. In fact, there is no definitive division between the two wedgebox

---

<sup>10</sup>Though the population structure within elements of the wedgebox plot will be altered.



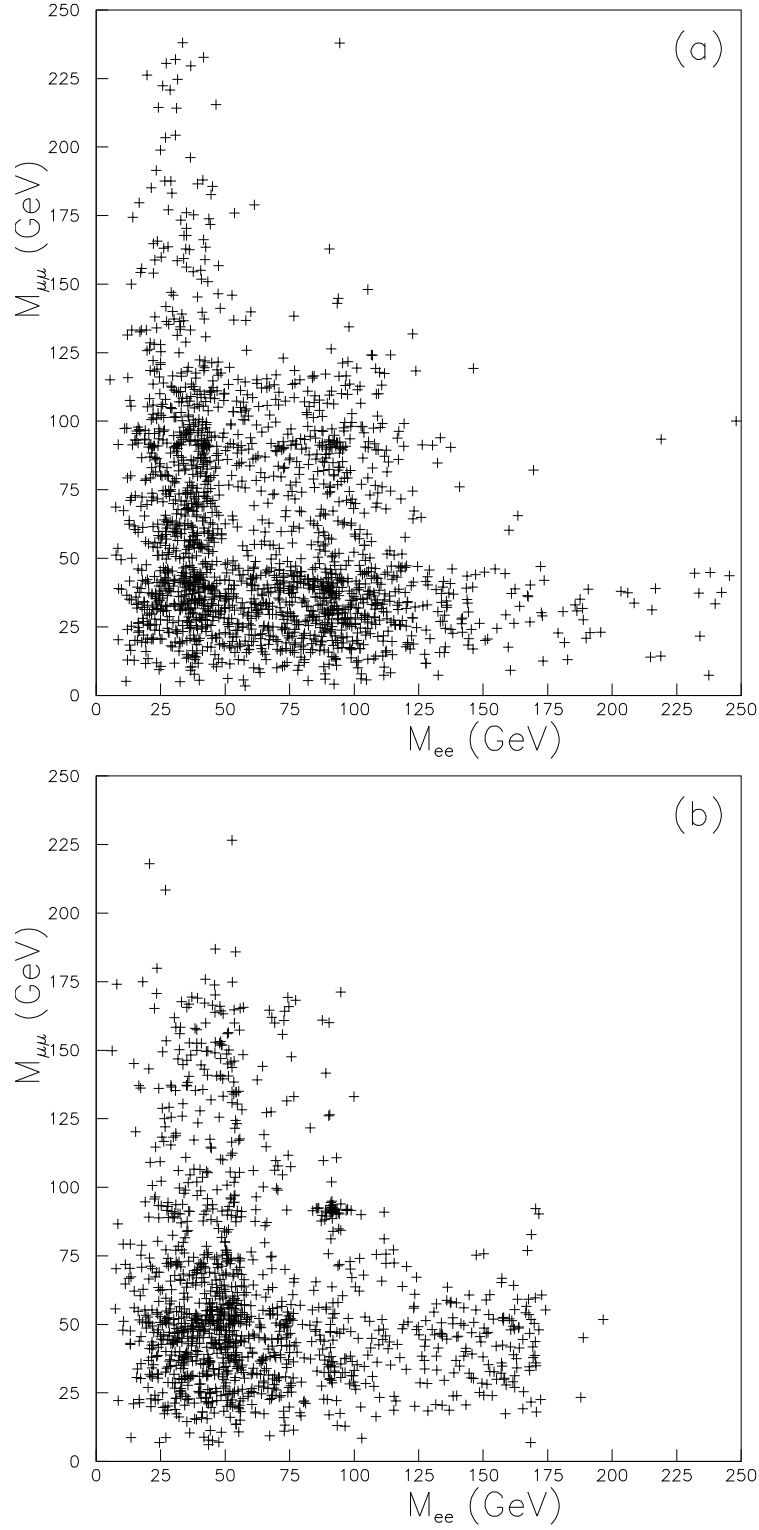


Figure 6: Wedgebox patterns for an integrated luminosity of  $300 \text{ fb}^{-1}$  at (a)  $(\mu, M_2) = (150 \text{ GeV}, 160 \text{ GeV})$  and (b)  $(\mu, M_2) = (190 \text{ GeV}, 280 \text{ GeV})$ ; in both cases  $\tan \beta = 20$ ,  $m_A = 600 \text{ GeV}$ , and  $m_{\tilde{\ell}_L} = m_{\tilde{\ell}_R} = 150 \text{ GeV}$ . All backgrounds remaining after cuts as described in the text are included. Bin size is  $2.5 \text{ GeV}$  along each axis.

shapes: quantitative criteria must be developed to gauge how many events are required to adequately resolve the outer edge of the longer wedge. For the moment visual inspection is all that is employed. In this double-wedge one may by eye identify  $M_{21}(\ell^+\ell^-) = 55 \pm 5$  GeV,  $M_{31}(\ell^+\ell^-) = 75 \pm 5$  GeV, and  $M_{41}(\ell^+\ell^-) = 175 \pm 10$  GeV. A more thorough analysis would of course employ a statistical likelihood analysis of these edges. It is already clear though the two-dimensional wedgebox plot offers a more precise method of edge-identification than the traditional one-dimensional projection as one can, for instance, see shifts between the edge locations along the axes in what would, in a one-dimensional plot, be taken as just one broader edge, and also discard some of the maverick events that fall outside the regular structures of the wedgebox plot. Further, anomalies in the population densities of structures presumed to be mirror images of each other along the two axes may become apparent. For the MSSM point plotted, the actual edges, calculable from the MSSM IPs, are  $M_{21}(\ell^+\ell^-) = 56.9$  GeV,  $M_{31}(\ell^+\ell^-) = 76.8$  GeV,  $M_{41}(\ell^+\ell^-) = 171.7$  GeV. on the muon side, and  $M_{21}(\ell^+\ell^-) = 56.6$  GeV,  $M_{31}(\ell^+\ell^-) = 76.9$  GeV,  $M_{41}(\ell^+\ell^-) = 172.6$  GeV on the electron side<sup>11</sup>. Agreement with the values above obtained from visual inspection is reasonable.

Though sub-dominant, a significant number of the events at points on the upper island still do arise from chargino production. For a quantitative estimate, a random sampling of non-Higgs-mediated events passing all cuts near the maximum of the second island was examined: 75% of these were direct neutralino production  $\tilde{\chi}_2^0\tilde{\chi}_3^0$  events yielding the expected inner wedge, while almost all the remaining events involved chargino production. Approximately half of the chargino events are ‘3+1’ events from chargino pair production, either  $\tilde{\chi}_2^\pm\tilde{\chi}_1^\mp$  or  $\tilde{\chi}_2^\pm\tilde{\chi}_2^\mp$ . The chargino yielding three leptons either decays via  $\tilde{\chi}_2^\pm \rightarrow \tilde{\chi}_2^0 W^\pm$  (with the  $W^\pm$  decaying leptonically), reinforcing the edges of the box in the lower left corner of the wedgebox plot, or via  $\tilde{\chi}_2^\pm \rightarrow Z^0\tilde{\chi}_1^\pm$ , leading to  $Z$ -lines on the wedgebox plot. The lighter chargino,  $\tilde{\chi}_1^\pm$ , decays over 90% of the time into a sneutrino and a single lepton, and the remaining < 10% of the time into a charged slepton and a neutrino, again yielding exactly one lepton. Almost all the remaining chargino events were from  $\tilde{\chi}_2^\pm\tilde{\chi}_{2,4}^0$  chargino-neutralino production. Here the  $\tilde{\chi}_2^\pm$  decays via  $\tilde{\chi}_2^\pm \rightarrow \tilde{\chi}_2^0 W^\pm$ , with the  $W^\pm$  decaying hadronically yet not leading to jets strong enough to violate the jet cut.

Fig. 7 (upper plot) shows the wedgebox plot for  $(\mu, M_2) = (190 \text{ GeV}, 280 \text{ GeV})$ , but this time with  $\tan\beta = 10$ . Note that the result is very similar to that with  $\tan\beta = 20$  seen in Fig. 6(b). In addition, Fig. 7 was made using the ISAJET 7.64 [5] event generator (coupled with a basic LHC detector simulation routine). Using ISAJET facilitates separating out the contributions from each production process. For this point in MSSM IP space, these are shown in the lower four plots of Fig. 7: the upper left plot is only from direct  $\tilde{\chi}_2^0\tilde{\chi}_3^0$  production, the upper right plot is from chargino production processes, and the lower left (right) plot is due to  $H^0$  ( $A^0$ ) production and subsequent decays. Halo events, as well as  $Z$ -lines, are clearly seen to

<sup>11</sup>This slight asymmetry arises from differences in the physical selectron and smuon masses which are due only to the fact that  $m_\mu \neq m_e$  — here  $m_{\tilde{\mu}_{L,R}}$  and  $m_{\tilde{e}_{L,R}}$  are left degenerate. See earlier comments though concerning the event generator.

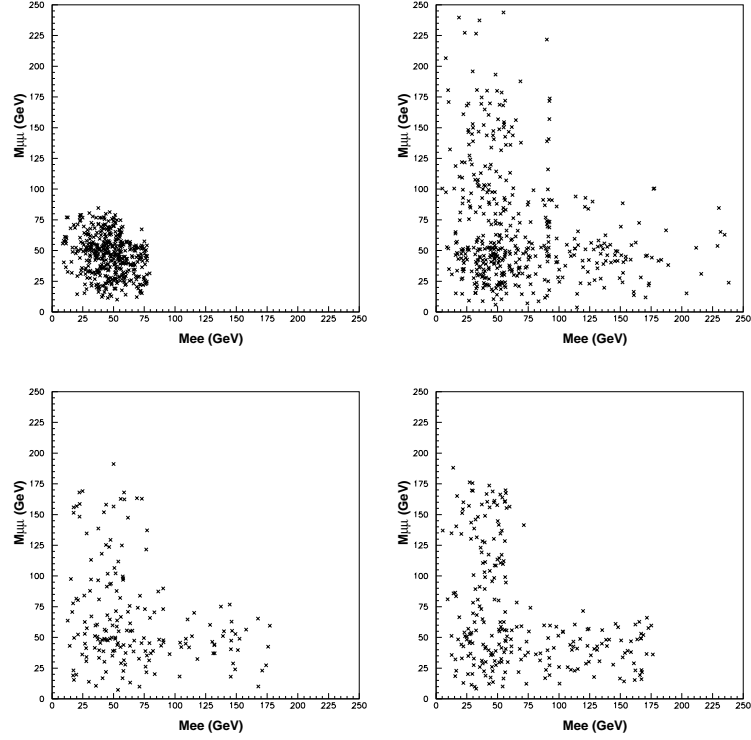
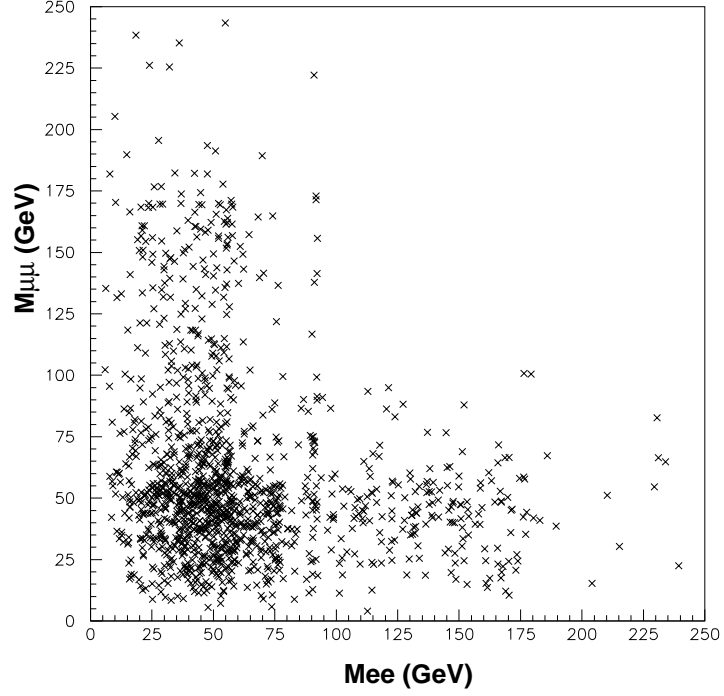


Figure 7: The wedgebox plot at  $(\mu, M_2) = (190, 280)$  and  $\tan \beta = 10$ , assuming an integrated luminosity of  $300 \text{ fb}^{-1}$  (center top); broken down into its  $\tilde{\chi}_2^0 \tilde{\chi}_3^0$  component (upper left),  $\tilde{\chi}_i^\pm \tilde{\chi}_j^\pm + \tilde{\chi}_i^\pm \tilde{\chi}_i^0$  component (upper right), and  $H^0, A^0$  components (lower left, right, respectively). Combining the components yields the double-wedge wedgebox plot (‘decorated’ by a halo and Z-lines from the chargino component) seen at the top. Note: this analysis was done using ISAJET [5].

come from the ‘maverick’ (‘3+1’) chargino events. Whereas  $\tilde{\chi}_2^0\tilde{\chi}_3^0$  production yields a clean, relatively short, wedge with an outer edge at  $\sim 80$  GeV, and  $H^0, A^0$  production gives a longer ( $\tilde{\chi}_2^0\tilde{\chi}_4^0$ ) wedge terminating around 175-180 GeV. A population change at around 75-80 GeV is also marginally discernible for the Higgs-mediated components. Note carefully that, although the chargino production plot is far from structureless, the edges of the (vaguely) wedge-like structure seen in this plot (a noticeable drop in the event population is apparent in the vicinity of 175 GeV) merely reinforce the edges seen in the  $H^0, A^0$  plots (and perhaps the  $\tilde{\chi}_2^0\tilde{\chi}_3^0$  plot as well), while the halo events and  $Z$ -line events do not prevent one from identifying the  $\tilde{\chi}_2^0\tilde{\chi}_3^0$  and  $H^0, A^0$  edges. This is true of all the upper island wedgebox plots examined: the maverick event characteristics do not obscure identification of the sought-after neutralino-based endpoints. The chargino-derived  $Z$ -line events do make the overall wedgebox plot look fatter, and one must be cautious not to be misled by mavericks which partially fill in the space between the  $Z$  lines and the wedges. Note that only the chargino-related component generates  $Z$ -lines. Adding effects from all these components produces a fairly easily-recognizable double-wedge.

As noted earlier, Fig. 5 is thus a representative example of a class of  $(\mu, M_2)$  wedgebox plots for one set of  $m_A, \tan\beta$  and slepton inputs. Now to examine variation within this class, first consider lowering  $\tan\beta$  from  $\tan\beta = 20$ : the total rate drops as seen in Fig. 3. However if a 30 event contour were added to each of the plots in Fig. 3, it would actually cover the entire region shown; thus, for an integrated luminosity of  $300 \text{ fb}^{-1}$  at the LHC, at least  $\sim 100$  events may be collected at all points shown for each  $\tan\beta$  value, sufficient to build a respectable wedgebox plot. Since it is really the Higgs boson processes which are losing rate while other processes are roughly constant, we expect wedgebox shapes at each point to remain more-or-less the same: on the lower island the minor Higgs boson contribution does not markedly affect the already complicated chargino-dominated wedgebox structure, while on the upper island removing the Higgs contribution at worst removes the edge associated with  $H/A \rightarrow \tilde{\chi}_2^0\tilde{\chi}_4^0$  (since  $H^0/A^0 \rightarrow \tilde{\chi}_2^0\tilde{\chi}_{2,3}^0$  simply reinforce edges already present from direct- and chargino-channels). So for lower  $\tan\beta$  values, it may not be possible to observe the double-wedge: somewhere between  $\tan\beta = 10$  and  $\tan\beta = 20$  the ‘300’ event (per  $100 \text{ fb}^{-1}$ ) contour vanishes, meaning it becomes questionable whether or not there is enough statistics to clearly identify the outer wedge of the double-wedge. Thus analogous plots to Fig. 5 for  $\tan\beta$  values of 5 or 10 look quite similar to the Fig. 5 save that more and more double-wedge wedgebox plots will become simple single-wedge wedgebox plots. As  $\tan\beta$  rises above 20, rates may continue to rise — if SUSY-breaking stau mass inputs are set safely above the corresponding selectron and smuon inputs, as has been done by hand here — or they may plummet (as noted earlier) — if stau inputs are made degenerate with those of the first two generations, in which case mixing will increasingly drive down one of the physical stau masses as  $\tan\beta$  grows, cutting down ‘leptonic’ (that is, electron and muon) BRs in favor of decays yielding taus.

The preceding paragraph touched upon the dependence of the appearance of Fig. 5 on inputs of the slepton sector, specifically, the value(s) of the stau inputs relative to those of the first two generations. Now, setting aside the staus for the moment,

consider how changing the selectron and smuon inputs will affect results. If the first two generations' degenerate input mass is raised above (lowered below) the nominal value of 150 GeV assumed in Fig. 5, all rates decline (grow). Repeating here the rough estimates given above, if rates fall significantly below 1000 events per  $300 \text{ fb}^{-1}$  at an upper island point in the MSSM IP space, double-wedge wedgebox plots tend to become single-wedge wedgebox plots, and if rates drop much below 100 events per  $300 \text{ fb}^{-1}$ , no clear wedgebox pattern may emerge at all. Thus by merely determining the overall event rate at a point and then referencing Fig. 5, a good estimate of what the wedgebox plot at that point should look like can often be deduced. If the degeneracy of the slepton mass inputs is lifted, then rates can be raised even if the left slepton inputs are made more massive, since the sneutrino masses also rise with the left slepton inputs, choking off the spoiler modes (see Fig. 4). If smuon SUSY-breaking mass inputs are pushed above those of the selectrons, rates may drop if significant non-sleptonic neutralino decay modes exist. In addition, the widths of the kinematical edges would shrink (anywhere from very modestly to enormously).

Lastly, consider the impact of altering  $m_A$ . This would affect the Higgs boson contributions (the focus of [2]) to the wedgebox plot. If  $m_A$  is lowered significantly, then the only open Higgs decay channel to neutralinos would be to  $\tilde{\chi}_2^0 \tilde{\chi}_2^0$ . This would produce a  $\tilde{\chi}_2^0 \tilde{\chi}_2^0$  box. If direct  $\tilde{\chi}_2^0 \tilde{\chi}_3^0$  production is significant, then the Higgs boson-induced  $\tilde{\chi}_2^0 \tilde{\chi}_2^0$  box would lie at the corner of the  $\tilde{\chi}_2^0 \tilde{\chi}_3^0$  wedge, producing no new edges and thus indistinguishable *by shape* from a wedgebox plot consisting solely of a  $\tilde{\chi}_2^0 \tilde{\chi}_3^0$  wedge. However, the presence of the Higgs boson-induced  $\tilde{\chi}_2^0 \tilde{\chi}_2^0$  box may well be noticeable via the population structure of the various component parts of the wedge — the Higgs boson decays in this case will over-populate the corner box of the wedge. The Higgs boson is critical to producing the very desirable double-wedge pattern, and, to allow this,  $m_A$  must be large enough to allow  $H^0$  and<sup>12</sup>  $A^0$  to decay to  $\tilde{\chi}_2^0 \tilde{\chi}_4^0$ . Yet if  $m_A$  is made too large, Higgs boson production rates drop off and the Higgs boson contribution dies. The event number estimate stated in the previous paragraph again can serve as a guide as to when clear double-wedge wedgebox plots may be identified.

## 4 Discussion

Fig. 8 shows the conventional one-dimensional projections which may be obtained from the two wedgebox plots in Fig. 6 by plotting both the  $M(e^+e^-)$  and the  $M(\mu^+\mu^-)$  values from each event along a single axis. While mass differences may still be inferred from sharp changes in curve (though care must be taken in interpreting, for instance, the maverick-induced glitch near 60 GeV in the upper plot or rate increases around the  $Z^0$  pole in both plots), information gained from correlating the  $M(e^+e^-)$  and  $M(\mu^+\mu^-)$  values is clearly lost, meaning that whether the events are generated chiefly by similar or dissimilar neutralino pair production may no longer be determined. Further, the ability to identify and thus exclude so-called ‘maverick’

---

<sup>12</sup>For larger values of  $m_A$  relevant here,  $H^0$  and  $A^0$  are nearly degenerate.

events outside of the wedge and box geometrical elements may significantly increase the purity of the sample events and the resulting resolution of the kinematical edges.

Two-dimensional wedgebox plots contain considerably more information often packaged in a manner readily understandable. For instance, a double-wedge or wedge-protruding-from-a-box wedgebox plot almost always<sup>13</sup> has edges corresponding to  $\tilde{\chi}_i^0 \rightarrow \tilde{\chi}_1^0$  decays ( $i = 2, 3, 4$  in order proceeding out along either axis). Though these values may not equal the neutralino mass differences, if the intermediate slepton or  $Z^0$  is on mass-shell (*cf.*, Eqn. 4), in any case much of information concerning the inputs to the MSSM neutralino mixing matrix and slepton sector may certainly be obtained. Technically, in other wedgebox patterns with fewer edges there is an inherent ambiguity in identifying the  $\tilde{\chi}_i^0 \rightarrow \tilde{\chi}_1^0$  decay responsible for each edge, though in practice taking the lowest available  $i$  for each edge is usually the correct choice; and the information concerning the MSSM input parameters extractable remains substantial.

Furthermore, commensurate with being able to compartmentalize the two-dimensional space of a wedgebox plot into a collection of simple geometrical shapes is the ability to examine the population densities in each element — for instance how many events would populate one leg of a wedge as compared to a box on the same wedgebox plot? Herein lies a true advantage of the wedgebox plot over the 1-dimensional projection. Theoretically, the distribution of the population of events within a given element is expected to be fairly simple, as noted in the introduction, at least before the implementation of cuts. Thus the expected the number of events in the corner box of a wedge versus the number in the legs is reasonably easy to estimate. This specifically allows us to tell whether Higgs boson  $H/A \rightarrow \tilde{\chi}_2^0 \tilde{\chi}_2^0$  production is present on top of a direct  $\tilde{\chi}_2^0 \tilde{\chi}_3^0$  channel-dominated wedge by virtue of the overpopulated corner box. Note this information is much harder to extract from a 1-dimensional projection.

In other analyses examining signals for the heavier MSSM Higgs bosons [2, 13] one typically selects a point in the MSSM IP space *and then* computes the signal rate from the Higgs boson(s) and the background rates from other MSSM processes<sup>14</sup>. Then if a large enough excess from the Higgs boson ‘signal’ is seen over the MSSM (+SM) ‘background’ a discovery or detection of the Higgs boson can be projected *at this point in the MSSM IP space*. But this raises the question, could the excess events attributed to the Higgs bosons at one point in the MSSM IP space be swallowed up by a larger SUSY background rate at another point in the MSSM IP space? This question is virtually never addressed, since in these studies it would be much too computationally impractical to find the background rates at an infinite number of points spanning the whole of MSSM IP space.

Contrast this with what may be inferred from the preceding studies connected with Fig. 5 and the variation of the MSSM IP parameters fixed to generate this

---

<sup>13</sup>This general rule can be broken by  $\tilde{\chi}_2^\pm \rightarrow \tilde{\chi}_1^\pm \ell^+ \ell^-$  decay events or by so-called ‘stripes’ (see [1]) where  $\tilde{\chi}_i^0 \rightarrow \tilde{\chi}_j^0 \ell^+ \ell^-$  ( $j \neq 1$ ). The former was mainly encountered in the region of the lower island and the latter was never found to be significant.

<sup>14</sup>Of course the SM backgrounds must also be considered, but these do not vary with the MSSM IPs.

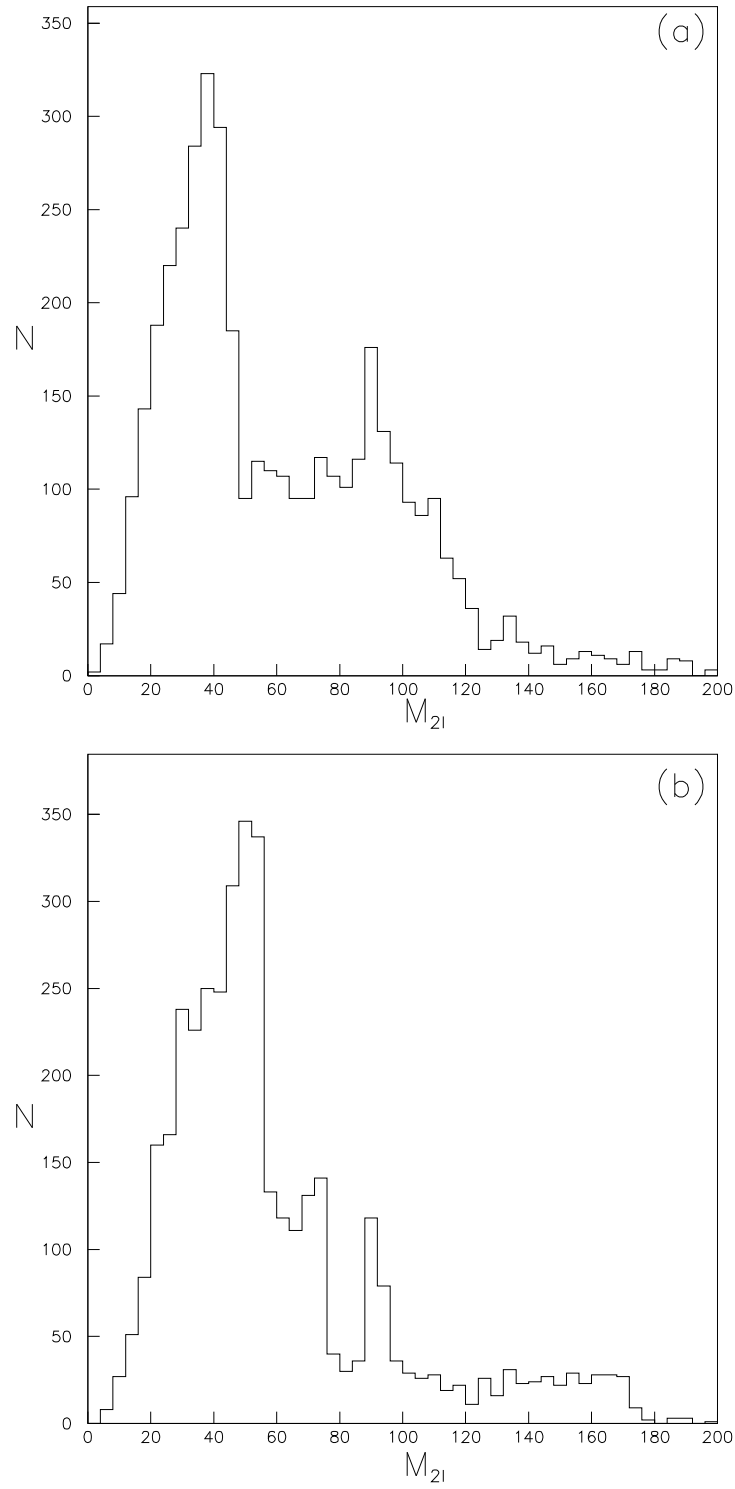


Figure 8: 1-dimensional projections of the two wedgebox plots in Fig. 6 obtained by putting values of both  $M(e^+e^-)$  and  $M(\mu^+\mu^-)$  for each event on one axis.

figure. Said studies indicate that all wedgebox maps should look similar to Fig. 5, except the distance from the islands' maxima where the number of events becomes too small to clearly identify any wedgebox pattern changes and, on the upper island<sup>15</sup>, double-wedge wedgebox plots shift into single-wedge wedgebox plots (or *vice versa*). The steadiness of the features in Fig. 5 allow several fairly robust conclusions to be drawn, within the context of the MSSM:

- any box-containing wedgebox plot (including patterns with an outer box envelope, patterns with a wedge protruding from a box (as in Fig. 6(a)), and patterns where a box is inferred through the over-population of the corner of a wedge) indicates that either Nature sits on the lower island in the lower corner of the  $(\mu, M_2)$  plane or events from  $H^0$  and  $A^0$  decays are present and substantial. The key here is the establishment that substantial direct neutralino pair production can only occur for  $\tilde{\chi}_2^0 \tilde{\chi}_3^0$  production, which yields a wedge not a box. Also it is crucial to exclude cascade processes via a sufficient cut on hadronic activity.
- The severity of the halo events, which stem from chargino and slepton production processes (especially '3+1' events), around the wedge and box geometries expected in the wedgebox theoretical framework indicates how near Nature lies to one of the axes. High levels of such contamination are found near the axes, for low  $\mu$  and/or  $M_2$  values, while, conversely, very 'clean' wedge like plots indicate moderate values of  $\mu, M_2$  ( $\sim 200$  GeV) and direct channel  $\tilde{\chi}_2^0 \tilde{\chi}_3^0$  domination.
- With rare exceptions, a double-wedge wedgebox plot unambiguously identifies three kinematical endpoints  $M_{i1}(\ell^+ \ell^-)$  ( $i = 2, 3, 4$ ) of neutralinos decaying through off-shell sleptons or  $Z^{0*}$ .

Ideally, one would like to make even stronger statements along the lines that if one sees a certain wedgebox pattern, this unambiguously means one is seeing evidence for the heavier MSSM Higgs bosons, regardless of the specific point in the MSSM IP space Nature has chosen. While the present analysis does not quite reach this goal, it is reasonable to expect that more detailed criteria can lead to definite conclusions concerning such issues. Nonetheless, the conclusions that may be drawn from the simple gross properties of wedgebox plots as herein presented is most encouraging. With the choices of where Nature might lie in the MSSM IP space narrowed down by such an analysis, the full weight of more intricate probing of the data (via neural network studies and their kin for instance) can optimize (though perhaps at the expense of clarity in the presentation of these results to those not immersed in the intricate details of hadron collider analyses of SUSY phenomenology) the amount of information extractable at the LHC.

Another handle that may aid in determining if heavy MSSM Higgs bosons are generating some of the  $e^+ e^- \mu^+ \mu^- + \cancel{E}$  events is the invariant mass of all four leptons

---

<sup>15</sup>The lower island is a domain of rapidly varying (as one moves around the IP space) wedgebox patterns which tend to be fairly complicated. This complexity serves to pinpoint the location in the parameter space as being on this lower island.



combined. This is expected to be bounded above by  $m_{H,A} - 2m_{\tilde{\chi}_1^0}$  [14]. However, the four-lepton (one-dimensional) invariant mass distribution will not have the abrupt turn off expected for the di-lepton invariant masses plotted in the wedgebox plot [14]. Studies suggest that the backgrounds and the low number of Higgs boson-generated events near the endpoint are likely to obscure detection of the endpoint. However, the shape of a histogram plotting the four-lepton invariant mass distribution may be markedly affected by having a significant fraction of the events coming from Higgs boson decays. Drawing conclusion from the distribution shape also encounters problems though since the shape of the MSSM background (as well as that of the Higgs boson signal) varies across the MSSM IP space, again leading to the unattractive methodology of first picking a point in the parameter space and then determining if the signal + background distribution differs significantly from the background alone distribution *at this point and this point alone* in the MSSM IP space. Conclusions drawn from the wedgebox plot may help to alleviate some of this uncertainty, enabling the four-lepton invariant mass distribution to be more successfully employed.

## 5 Conclusions

The wedgebox technique may be used to effectively and elegantly categorize any positive outcome of an LHC search for the  $e^+e^-\mu^+\mu^- + \cancel{E}$  signature expected from MSSM neutralino pair production. A search of the entire available MSSM IP space reveals that a sufficient number of events to make a viable wedgebox plot (somewhat arbitrarily set as being  $> 100$  assuming an integrated luminosity of  $100\text{ fb}^{-1}$ ) is obtained only on two ‘islands’ in the  $(\mu, M_2)$  plane (as shown in Fig. 3). Here it is assumed slepton masses are relatively low with  $m_{\tilde{\ell}_L} \simeq m_{\tilde{\ell}_R}$  — if this equality is altered, then the strengthening (weakening) of sneutrino spoiler modes tends to make the islands sink (the moat between the islands dry up) for  $m_{\tilde{\ell}_L} < (>) m_{\tilde{\ell}_R}$ .

Much of the lower island is already excluded by negative search results at LEP. Signature events on the small as-of-yet unexcluded portion of this island result from a smorgasbord of different production processes including a large, even dominant, component from processes involving charginos. Not unexpectedly, a plethora of wedgebox plot patterns result, with one pattern shifting into another fairly rapidly as the exact location in the MSSM IP space shifts. A weakness of the wedgebox plot technique is that it does not fully include charginos into its theoretical framework (at least not thus far). What can be said is that if a wedgebox plot with a complicated structure is observed, then this points toward Nature resting on this small portion of this lower island. It would be quite a coup if this were observed, and would no doubt motivate more detailed examinations to pry more information from the rich though complicated characteristics of this MSSM IP region.

The last statement is possible because of the simple character of the larger upper island: here the wedgebox pattern is remarkably constant, consisting either of a single- or double-wedge. This is mostly due to the fact that the only neutralino pair to be directly produced at any appreciable rate is  $\tilde{\chi}_2^0\tilde{\chi}_3^0$ , and this yields a wedge pattern. Furthermore, unlike on the lower island, chargino production processes on

the upper island are of a more tame variety, and mostly fortify the wedge structure (though halo events and sometimes  $Z$ -lines are added to the underlying wedgebox structure one hopes to categorize), while slepton backgrounds are negligible. The clarity of the double-wedge pattern on the upper island depends on whether Higgs-mediated neutralino pair production yields a sufficient number of  $\tilde{\chi}_2^0 \tilde{\chi}_4^0$  events for detection of the kinematical edge resulting from  $\tilde{\chi}_4^0 \rightarrow \tilde{\chi}_1^0 \ell^+ \ell^-$  decays. Therefore if the MSSM IPs are tuned to give a very clear double-wedge pattern (*i.e.*, at the level of Fig. 6(b) or better), or a wedge-protruding-from-a-box pattern, then one can directly read off the kinematic edges  $M_{i1}(\ell^+ \ell^-)$ , ( $i = 2, 3, 4$ ), which strongly constrain the neutralino and slepton spectra and the corresponding MSSM IPs.

Another fairly sweeping general result emerges from studying the variation of the wedgebox plot patterns across the MSSM IP space: the presence of a box in a wedgebox plot, where hadronically noisy events from gluino and squark cascade decays have been removed, signals either chargino production or heavy Higgs boson-mediated neutralino pair production, where the former only generates suitably-resolved boxes in the quite restricted region of the MSSM IP space around  $\mu, M_2 \lesssim 200$  GeV (the location of the lower island). Here boxes include box-like outer envelopes to the wedgebox pattern, boxes with wedges protruding from them, and boxes identified via over-populated lower-left corners of wedges. Compare this result to analyses that attempt to prove the presence of heavy Higgs bosons by looking for excesses in the number of expected background events from SM *and other MSSM processes* on the basis of point-by-point studies in the MSSM IP space. What, other than further *typically unspecified* analyses, is to say that the excess attributed to Higgs bosons at one point studied in the IP space could not be due to larger background MSSM process rates at some other unstudied point in the IP space?

We note the above conclusions are justifiable only by the ability to distinguish correlations between  $M(e^+ e^-)$  and  $M(\mu^+ \mu^-)$  in the wedgebox technique<sup>16</sup>, this being manifestly impossible in the more traditional 1-dimensional invariant mass histograms like those shown in Fig. 8. Other advantages of this technique include (1) there is a one-to-one correspondence between an four-lepton event and a point on the plot, (2) asymmetries between slepton generations can be observed, and (3) better resolution of kinematic edges is possible by way of cutting out maverick and  $Z$ -line events which protrude from the dominant wedgebox shape.

The method therefore represents a technical improvement. Though it must be cautioned that this does not imply that the technique is guaranteed to unambiguously determine the presence of the heavier MSSM Higgs bosons, or yield a double-wedge wedgebox pattern from which loads of information on MSSM IPs can be mined, or restrict said MSSM IPs to the lower island by the complexity of the observed wedgebox plot. Regrettably, at many points in the MSSM IP space, the  $e^+ e^- \mu^+ \mu^- + \cancel{E}$  signal rate is too low to construct a wedgebox plot (see footnote 16 for a partial remedy for this though). It is perhaps also useful to bear in mind that Nature will

---

<sup>16</sup>It also appears possible [8] to use  $e^+ e^- e^+ e^-$  and  $\mu^+ \mu^- \mu^+ \mu^-$  events and use relatively simple criteria to correctly (a high percentage of the time) pair up the leptons. This will approximately double the event rates.

select out one and only one point in the MSSM IP space. And Nature may not chose to pay any attention to statements about what is true over large stretches of the IP space in making said selection.

Finally, note that this technique can be used to compare outputs expected in various different sub-spaces of the MSSM IP space, such as those resulting from specifying different SUSY-breaking mechanisms (*e.g.*, mSUGRA or GMSB) and associated higher energy-scale features of the model. It can also be applied to the NMSSM, which adds a fifth neutralino, to little Higgs (extra-dimensions) models with T-parity [15] (KK-parity [16]), or indeed (as noted in [1]) to any model in which heavy exotic particles  $X_i$  decay to dilepton pairs  $X_i \rightarrow \ell^- \ell^+$  and there is more than one  $X_i$ . To ascertain the potential usefulness of the wedgebox technique in such models a wedgebox map or maps may be constructed covering the relevant parameter space.

## References

- [1] M. Bisset, N. Kersting, J. Li, F. Moortgat, S. Moretti and Q.L. Xie, Eur. Phys. J. C **45** (2005) 477.
- [2] M. Bisset, N. Kersting, J. Li, F. Moortgat and S. Moretti, work in progress.
- [3] H. Bachacou, I. Hinchliffe and F.E. Paige, Phys. Rev. D **62** (2000) 015009.
- [4] H. Baer and X. Tata, Phys. Rev. D **47** (1993) 2739.
- [5] H. Baer, F.E. Paige, S.D. Protopopescu and X. Tata, hep-ph/0001086, hep-ph/0312045.
- [6] W.-M. Yao *et al.* (Review of Particle Physics, page 1127), J. Phys. G: Nucl. Part. Phys., **33** (2006) 1.
- [7] H.E. Haber and G.L. Kane, Phys. Rep. **117** (1985) 75.
- [8] G. Bian, M. Bisset and N. Kersting, work in progress.
- [9] G. Corcella *et al.*, JHEP **0101** (2001) 010, hep-ph/0210213; S. Moretti, K. Odagiri, P. Richardson, M.H. Seymour and B.R. Webber, JHEP **0204** (2002) 028.
- [10] J. Pumplin *et al.* (CTEQ Collaboration) (CTEQ6), JHEP **0207** (2002) 012, *ibid*, **0310** (2003) 046; H.L. Lai *et al.* (CTEQ Collaboration) (CTEQ5), Eur. Phys. J. C **12** (2000) 375.
- [11] See:  
<http://www-thphys.physics.ox.ac.uk/users/PeterRichardson/HERWIG/isawig.html>.
- [12] A. Djouadi, J. Kalinowski and M. Spira, Comput. Phys. Commun. 108, 56 (1998).

- [13] M. Bisset, F. Moortgat and S. Moretti, Eur. Phys. J. C **30** (2003) 419.
- [14] H. Baer, M. Bisset, D. Dicus, C. Kao and X. Tata, Phys. Rev. D **47** (1993) 1062;  
H. Baer, M. Bisset, C. Kao and X. Tata, Phys. Rev. D **50** (1994) 316.
- [15] H.-C. Cheng and I. Low, JHEP **0309** (2003) 051, JHEP **0408** (2004) 061; J. Hubisz and P. Meade, Phys. Rev. D **71** (2005) 035016.
- [16] H.-C. Cheng, K.T. Matchev and M. Schmaltz, Phys. Rev. D **66** (2002) 056006.